Journal of the European Ceramic Society xxx (xxxx) xxx

Contents lists available at ScienceDirect

Journal of the European Ceramic Society

journal homepage: www.elsevier.com/locate/jeurceramsoc

Sintering temperature, microwave dielectric properties and structural characteristics of $Li_2Zn_6MgTi_6O_{20}$ ceramic with high configuration entropy

Qianbiao Du, Jianhong Duan, Linzhao Ma, Longxiang Jiang, Hao Li *

College of Electrical and Information Engineering, Hunan University, Changsha, Hunan 410082, China

ARTICLE INFO

Keywords:
Disordered state
Microwave dielectric properties
P–V–L theory
High configuration entropy

ABSTRACT

The novel spinel $Li_2Zn_6MgTi_6O_{20}$ ceramic with high configuration entropy was synthesized using the traditional solid-state method. Analysis from X–ray diffraction, transmission electron microscope, and Raman spectra demonstrates a disordered state in $Li_2Zn_6MgTi_6O_{20}$ (*Fd-3m*). This dense ceramic exhibits excellent microwave dielectric properties at 1240 °C: $\varepsilon_r = 18.01 \pm 0.2$, $Q\times f = 98{,}450 \pm 3{,}000$ GHz (at 9.17 GHz), and $\tau_f = -38 \pm 3.6$ ppm/°C. Further studies combining bond valence and P–V–L theory reveal that Ti^{4+} significantly influences the ε_r of $Li_2Zn_6MgTi_6O_{20}$ ceramic, while the Ti^{4+} polarizability is underestimated by 10.6%, resulting in the ε_r higher than the ε_{th}. The solid solution leads to structural disorder and high configuration entropy, driving each bond to contribute almost equally to the bond energy. This structural feature promotes a favorable and stable microstructure, enhancing the microwave dielectric and sintering properties synergistically. Furthermore, the τ_f is optimized by composites (—4.5 ppm/°C).

1. Introduction

Microwave dielectric ceramics are commonly used in the production of passive devices such as resonators, filters, antennas, and substrates, among other key materials. They play an increasingly important role in the field of modern communication [1–3]. Excellent microwave dielectric properties including an appropriate dielectric constant (ε_r), a high quality factor ($Q\times f$), and a near-zero resonant frequency temperature coefficient (τ_f), are crucial indicators for evaluating the practicality and advancement of these materials [4–6].

Recently, Ti-based microwave dielectric ceramics have seen significant development and application in recent years due to their excellent microwave dielectric properties and good sintering temperature, such as commercial $MgTiO_3$-$CaTiO_3$ system ceramics [7], Li_2TiO_3 system [8], Li_2O-MgO-TiO_2 system [9], and spinel-structured Mg_2TiO_4 [10], $Li_4Ti_5O_{12}$ [11]. Among them, Zn_2TiO_4, a spinel structure with a space group *Fd-3m* extremely resembling Mg_2TiO_4, has great potential as a microwave dielectric ceramic. Nevertheless, compared to Mg_2TiO_4, Zn_2TiO_4 exhibits less ideal microwave dielectric properties, with a suboptimal $Q\times f$ (50,000 GHz) at temperatures below 350 °C, a ε_r of 21, and a large negative τ_f (—60 ppm/°C) [12]. Li *et al.* [13] replaced the Mg^{2+} position in Mg_2TiO_4 ceramics with Zn^{2+} and found that $ZnMgTiO_4$ exhibited a superb $Q\times f$ value (202,021 GHz) at 1400 °C. However, at a further temperature of 1420 °C, $ZnMgTiO_4$ decomposed and formed the second phase, $MgTiO_3$. Another promising option is the ordered structure of $Li_2MTi_3O_8$ (M= Zn, Mg, Co, Ni) ceramics, which exhibit a cubic spinel structure [14–16]. They are not only characterized by low sintering temperatures (950 ℃-1075 ℃), but also have excellent microwave dielectric properties, especially exhibiting near-zero τ_f values. Specifically, $Li_2ZnTi_3O_8$ ceramics exhibit excellent microwave dielectric properties $\varepsilon_r = 25.6$, $Q\times f = 76{,}000$ GHz, and $\tau_f =$ —12 ppm/°C at 1075 °C.

In recent years, high-entropy materials with multiple elements occupying equivalent lattice sites have attracted attention due to their enhanced properties resulting from entropy-dominated phase stabilization, lattice distortion caused by structural disorder, slow diffusion kinetics, and the synergistic effects of multicomponent properties in fields such as electrostatic dielectric capacitors [17], batteries [18], and catalysts [19]. Notably, certain researchers have achieved excellent microwave dielectric properties by designing high-entropy ceramics, such as $(Hf_{0.25}Zr_{0.25}Sn_{0.25}Ti_{0.25})O_2$ [20] and $(La_{0.2}Nd_{0.2}Sm_{0.2}Ho_{0.2}Y_{0.2})(Nb_{1-x}V_x)O_4$ [21]. The atomic configuration entropy (S_{config}) is defined by

$$S_{config} = -R\left(\left(\sum_{i=1}^{N} x_i \ln x_i\right)_{cation-site} + \left(\sum_{j=1}^{M} x_j \ln x_j\right)_{anion-site}\right) \quad (1)$$

* Corresponding author.
E-mail address: haouestc@gmail.com (H. Li).

https://doi.org/10.1016/j.jeurceramsoc.2024.02.058
Received 2 January 2024; Received in revised form 23 February 2024; Accepted 28 February 2024
Available online 2 March 2024

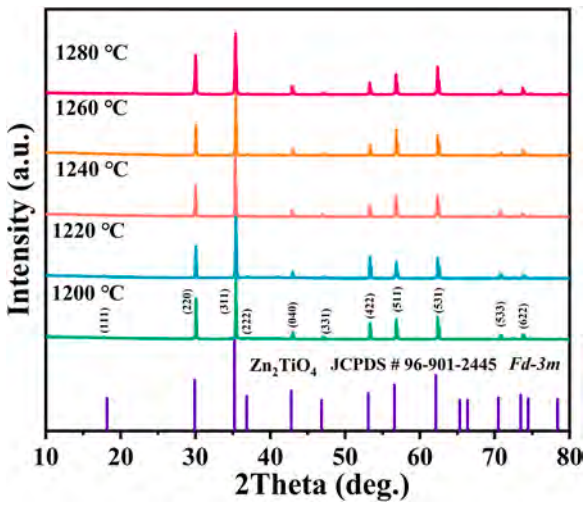

Fig. 1. XRD patterns of $Li_2Zn_6MgTi_6O_{20}$ ceramics sintered at 1200 ℃ - 1280 ℃.

Where R, $N(M)$, and x_i (x_j) refer to the ideal gas constant. To introduce conformational entropy, we explore building the ternary system Zn_2TiO_4-$ZnMgTiO_4$-$Li_2ZnTi_3O_8$ ($Li_2Zn_6MgTi_6O_{20}$, $S_{config} = 1.09\,R$). Through synergistic effects, we achieved microwave dielectric ceramics with excellent comprehensive properties, effectively addressing the limitations of the original ceramics.

In this work, $Li_2Zn_6MgTi_6O_{20}$ ceramics were prepared by the solid-state method to explore the relationship between phase composition, structure, and microwave dielectric properties. The work also tuned its τ_f to zero through phase composite methods to promote the practical application of ceramics. The Phillips-Van Vechten-Levine (P–V–L) chemical bond theory was also used to establish the relationship between the chemical bond characteristics and microwave dielectric properties.

2. Experimental procedures

The high purity raw materials, ZnO (> 99.90%, Aladdin), Li_2CO_3 (> 99.90%, Aladdin) and TiO_2 (> 99.9%, Aladdin) of $Li_2Zn_6MgTi_6O_{20}$ ceramics were weighed in stoichiometric ratios and ball-milled with anhydrous ethanol for 10 hours. The resulting powders were dried at 100 °C for 2 h and calcined in a muffle furnace at 800 °C for 6 h. The calcined powders underwent a second round of ball milling for 10 hours using the same conditions as before, resulting in a finer and more homogeneous powder. After drying, the powders were mixed with 5 wt% polyvinyl alcohol (PVA) to form granules. These granules were then pressed into cylindrical columns measuring 10 mm in diameter and 6 mm in height. Subsequently, the samples underwent a sintering process in a muffle furnace, with temperatures ranging from 1200 °C to 1280 °C (the heating rate is 5 °C/min). Prior to the sintering process, a calcination step was carried out at 550 °C to eliminate the organic matter PVA (the heating rate is 1.5 °C/min).

X-ray diffraction (XRD, Philips, X′pert Pro MPD, Netherlands) with a detection range of 10°–120° was used to identify the physical phase. The details of the structural changes induced by component variations were further explored by Rietveld structure refinement using Fullprof software based on XRD data. The transmission electron microscope (TEM, JEOL JEM-2100 F, Tokyo, Japan) was utilized to acquire both the selected area electron diffraction (SAED) patterns and high-resolution transmission electron microscopy (HRTEM) images. The SAED patterns and HRTEM images were captured to examine the structural characteristics of the samples at a high resolution. $Li_2Zn_6MgTi_6O_{20}$ samples were polished to a mirror finish using a polishing machine (UNIPOL-802) and then subjected to thermal etching at a temperature 50 °C below the sintering temperature for 30 minutes. The microscopic morphology of the samples was examined using a scanning electron microscope (SEM, FEI, Quanta FEG250, USA). The determination of grain sizes was carried out by measuring the linear intercept method. Raman spectra were performed using a Raman scattering spectrometer (Renishaw, inVia™, UK). The determination of ε_r and $Q\times f$ values was carried out using the Hakki-Coleman method (TE011 mode) with the assistance of a network analyzer (Agilent Technologies E5071C). A temperature chamber at 25 °C-85 °C was used to determine the τ_f value of the ceramics. τ_f was calculated by formula (2) [22]:

$$\tau_f = \frac{f_{85} - f_{25}}{(85-25)f_{25}} \tag{2}$$

The resonant frequencies at 85 °C and 25 °C were denoted by f_{85} and f_{25}, respectively.

3. Results and discussions

The XRD patterns of $Li_2Zn_6MgTi_6O_{20}$ ceramics at different temperatures (1200 °C - 1280 °C) are represented in Fig. 1. The diffraction peaks of all the samples match well with the standard card of Zn_2TiO_4 (JCPDS # 96–901–2445), and no additional diffraction peaks can be detected, which demonstrates that $Li_2Zn_6MgTi_6O_{20}$ ceramic generates a cubic spinel phase with a space group of *Fd*-3*m*. Additionally, the Rietveld refinement by the Fullprof program was conducted to further explore the detailed information on the crystal structure of $Li_2Zn_6MgTi_6O_{20}$ ceramic. Fig. 2(a) shows the observed and calculated result

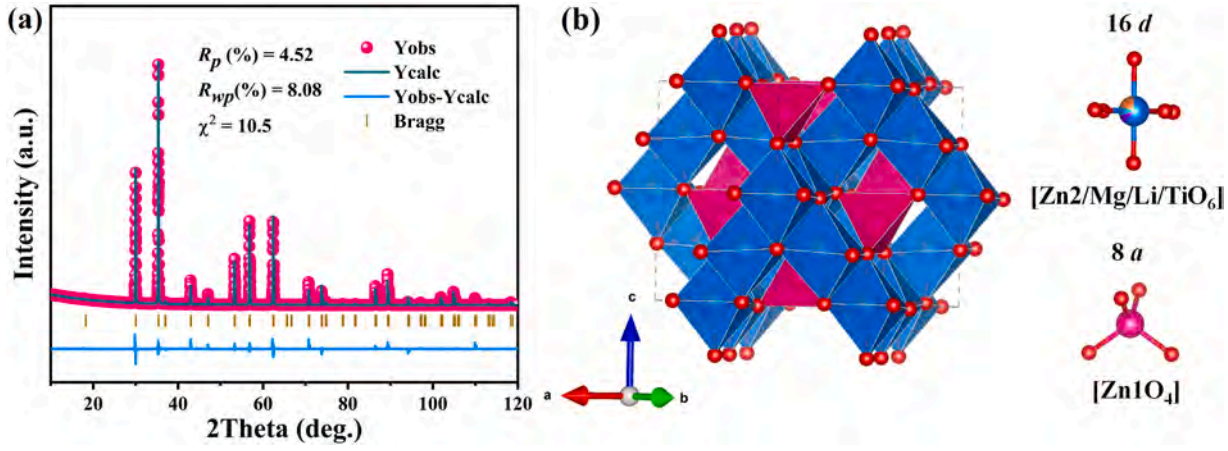

Fig. 2. (a) Rietveld refinement result profiles of XRD data for $Li_2Zn_6MgTi_6O_{20}$ ceramic sintered at 1240 ℃; (b) Schematic diagram of the crystal structure of $Li_2Zn_6MgTi_6O_{20}$.

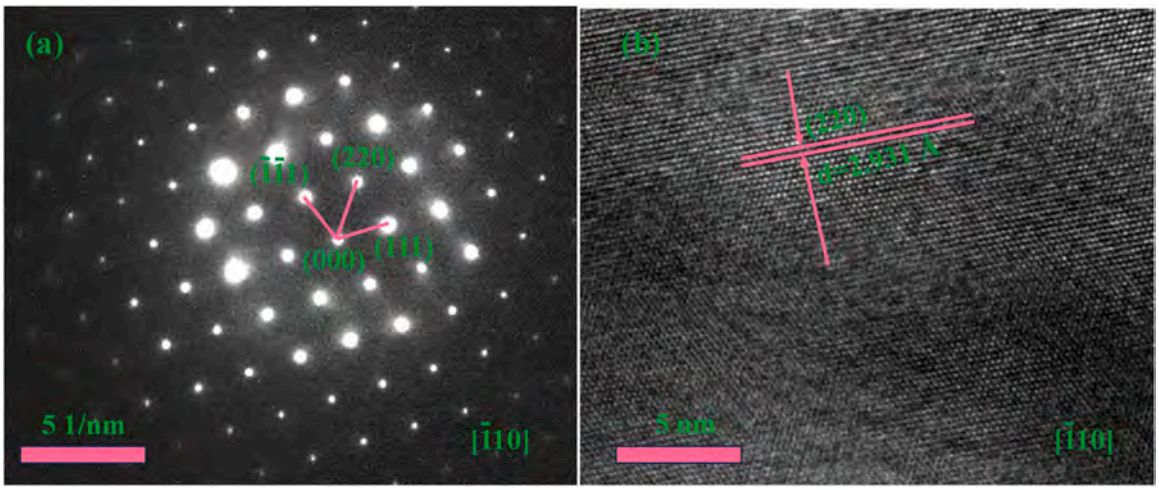

Fig. 3. SAED and HRTEM images of $Li_2Zn_6MgTi_6O_{20}$ ceramics taken along the [_110] zone axes at room temperature.

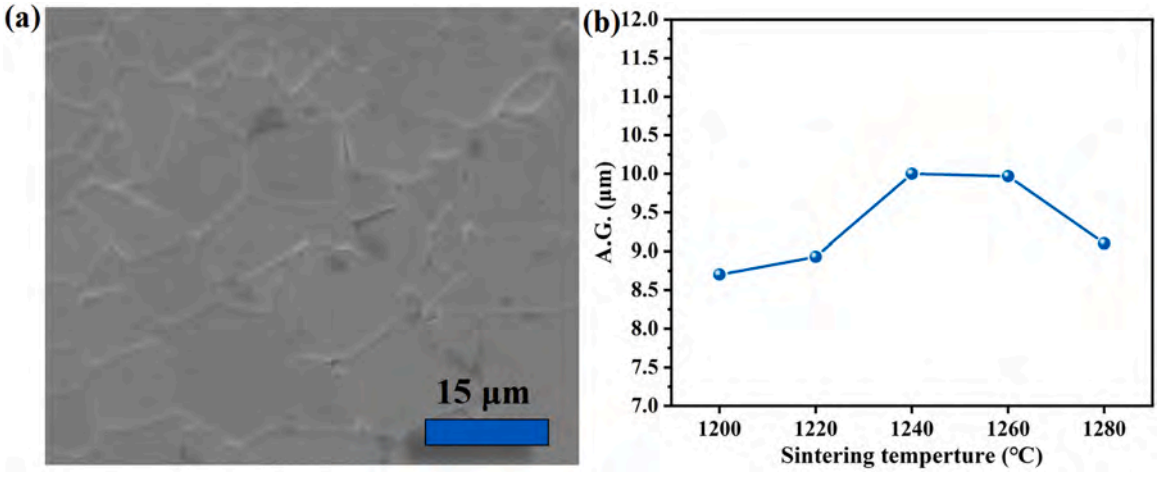

Fig. 4. (a) SEM images of polished and thermally etched $Li_2Zn_6MgTi_6O_{20}$ ceramic sintered at 1240 °C, (b) Average grain size of $Li_2Zn_6MgTi_6O_{20}$ ceramics at 1200–1280 °C.

profiles of $Li_2Zn_6MgTi_6O_{20}$ ceramic at 1240 °C based on the Zn_2TiO_4 model, along with fine reliability factors (R_p, R_{wp}, and χ^2). The lattice parameters of $Li_2Zn_6MgTi_6O_{20}$ ceramic sintered at 1240 °C are $a = b = c = 8.4158$ Å, and $V = 596.059$ Å^3. Table S1 lists the crystallographic details of the atoms in the crystal structure of $Li_2Zn_6MgTi_6O_{20}$. Based on the refined results, a schematic diagram of the unit cell structure of $Li_2Zn_6MgTi_6O_{20}$ ceramic is obtained in Fig. 2(b). The crystal structure of $Li_2Zn_6MgTi_6O_{20}$ ceramic closely resembles that of Zn_2TiO_4. Zn^{2+} prefers to occupy the 8*a* site, forming a tetrahedron configuration, which is in line with the low octahedral site preference energy (OSPE) of only 0 kcal/mol. The remaining cations, including Zn^{2+}, Li^+, Mg^{2+}, and Ti^{4+}, are randomly distributed in the 16*d* site, forming octahedra with a disordered atomic arrangement. This disordered structure, which contributes to higher entropy values, has an important effect on the microwave dielectric properties of ceramics. And based on such atomic occupancy information and the effective radii of the cations ($R_{Zn2+} = 0.74$ Å, $R_{Mg2+} = 0.72$ Å, $R_{Li+} = 0.76$ Å, $R_{Ti4+} = 0.605$ Å), a significant lattice contraction at the B site can be found ($R_{av} = 0.6610$ Å) compared to Zn_2TiO_4 ($R_{av} = 0.6725$ Å). This is also a major reason why the unit cell volume of $Li_2Zn_6MgTi_6O_{20}$ ceramics is smaller than that of Zn_2TiO_4 ceramics ($V = 607.232$ Å^3) [23].

SADE and HRTEM patterns of $Li_2Zn_6MgTi_6O_{20}$ ceramic are used to further investigate the crystal structure information. As shown in Fig. 3 (a), the diffraction spots of SADE along the zone axis [_110] are exclusively conformed to the disordered structure of cubic spinel *Fd*-3*m* phase. Furthermore, in the HRTEM pattern, along the same zone axis, an identical crystal plane (220) with a crystal plane spacing (*d*) of 2.931 Å is identified. These results are well consistent with the results of the XRD data.

The SEM image of the thermally etched $Li_2Zn_6MgTi_6O_{20}$ ceramic at a densification temperature of 1240 °C is shown in Fig. 4(a), along with details of the grain distribution in Fig. S1. It's evident that the $Li_2Zn_6MgTi_6O_{20}$ ceramic exhibits a dense and uniform microstructure. Fig. 4 (b) shows the average grain size (A.G.) of the ceramics at various temperatures. As the temperature increases, the grains rapidly grow, reaching an average size of 10 μm at 1240 °C. Subsequently, with further temperature increases, non-uniform growth begins to occur, resulting in a decrease in A.G.

Fig. 5(a) shows the temperature effect on the bulk density and relative density of $Li_2Zn_6MgTi_6O_{20}$ ceramic. The bulk density and relative density of $Li_2Zn_6MgTi_6O_{20}$ ceramic at the densification temperature (1240 ℃) are 4.46 cm/℃ and 96.4%, respectively. Temperature has a significant effect on $Li_2Zn_6MgTi_6O_{20}$ ceramic. This is consistent with the SEM results presented in Fig. 4. By increasing the temperature to 1220 °C, the relative density increases rapidly to over 95%. The decrease in density afterwards may be affected by the volatilization of Li in addition to the sintering temperature.

Fig. 5(b-d) represents the effect of sintering temperature on the

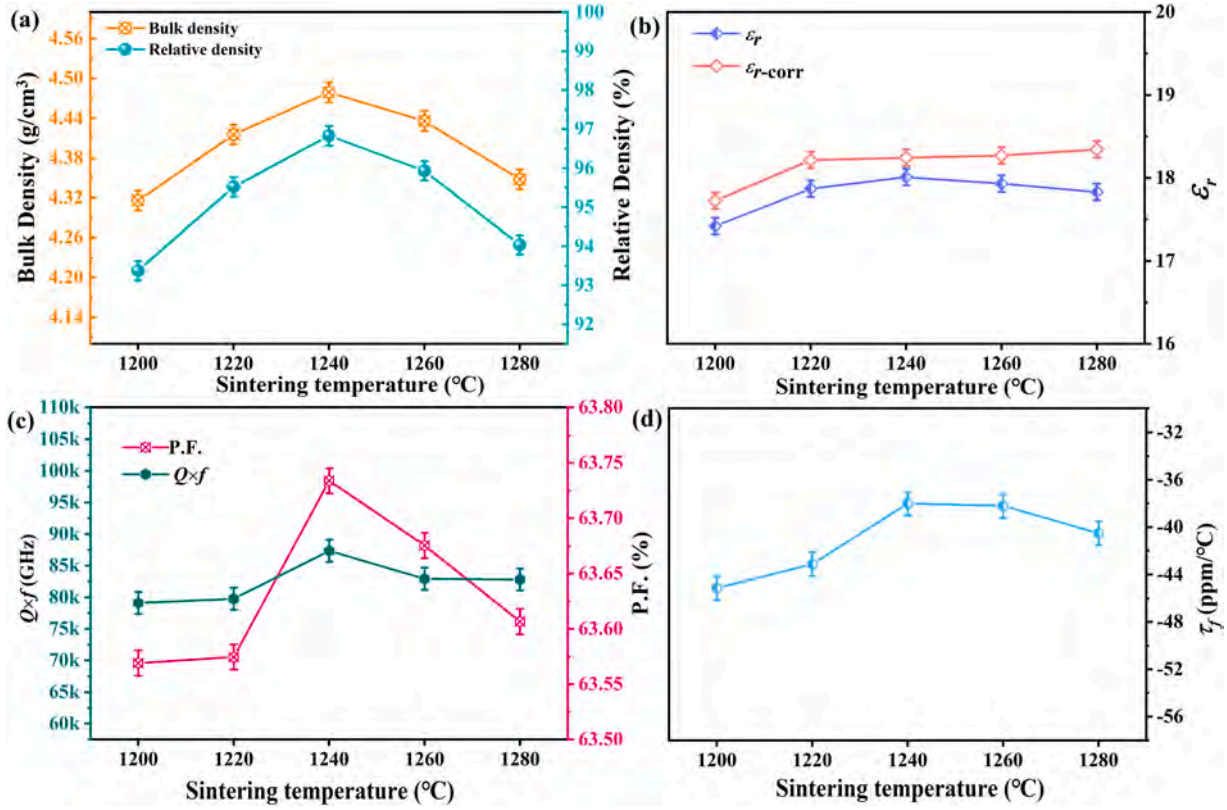

Fig. 5. The ε_r, $Q \times f$ and packing fraction, τ_f for the ceramic $Li_2Zn_6MgTi_6O_{20}$.

Table 1
bond valence and bond length of B site in $Li_2Zn_6MgTi_6O_{20}$ ceramic.

Bond	Bond valence	Bond length	f_i (%)
Zn1-O	1.466	1.9827	53.32
Zn2-O	2.585	2.0155	76.56
Mg-O	2.510		76.56
Li-O	1.359		57.03
Ti-O	3.490		88.33

microwave dielectric properties of $Li_2Zn_6MgTi_6O_{20}$ ceramics. Similar to the trend of the relative density of ceramics, the dielectric constant of $Li_2Zn_6MgTi_6O_{20}$ ceramics shows a rapid increase from 17.42 with increasing temperature until it reaches a peak of 18.01 at 1240 °C. As the temperature continues to increase, the ε_r tends to decrease. This change stems primarily from changes in the densification of the ceramics. The change in relative density suggests that temperature induces the creation of porosity and changes in cell volume, which will have a significant effect on the ε_r of the ceramic. Firstly, the ε_r is corrected to exclude the effect of porosity on the dielectric constant by the following equation [24].

$$\varepsilon_r = \varepsilon_{r-corr} \left(1 - \frac{3P(\varepsilon_{corr} - 1)}{2\varepsilon_{corr} + 1}\right) \quad (3)$$

where P refers to the porosity fraction of the sintered ceramic, $\varepsilon_{r\text{-}corr}$ is the corrected ε_r. At the densification temperature of 1240 °C, the value of $\varepsilon_{r\text{-}corr}$ is 18.24. From Fig. 5(b), it's clear that as the temperature increases, the difference between ε_r and $\varepsilon_{r\text{-}corr}$ becomes narrower and then wider. This indicates that temperature plays an important role in the ε_r

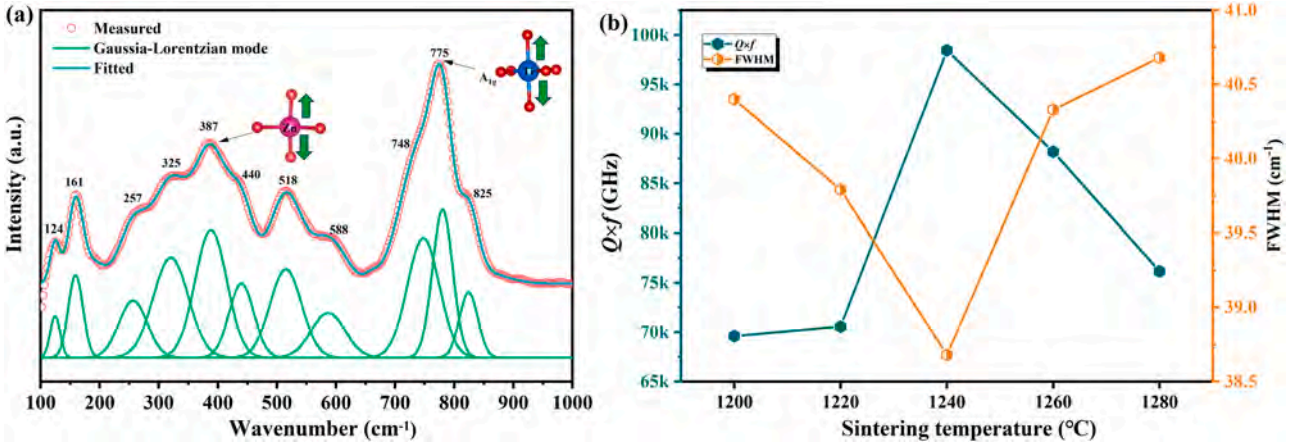

Fig. 6. (a) The room-temperature Raman spectra with Raman Gaussian Lorentz fit of $Li_2Zn_6MgTi_6O_{20}$ ceramic; (b) $Q \times f$ and FWHM.

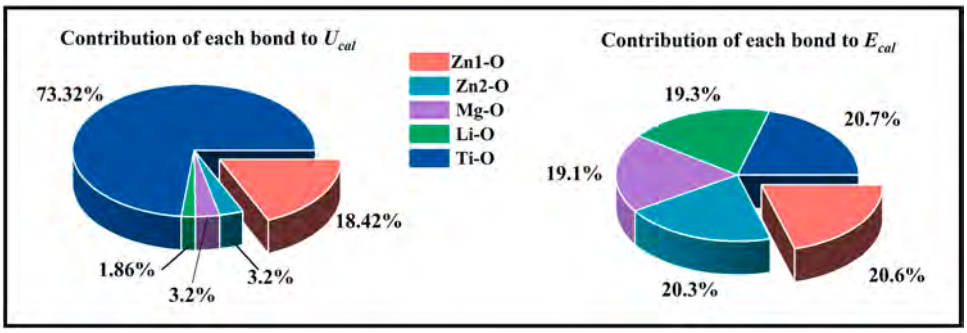

Fig. 7. Ratio of individual bond contributions to U and E in $Li_2Zn_6MgTi_6O_{20}$ ceramic.

of $Li_2Zn_6MgTi_6O_{20}$ ceramic. In addition, the theoretical dielectric constant (ε_{th}) of $Li_2Zn_6MgTi_6O_{20}$ ceramics can be obtained by the Clausius–Mosotti equation [25]. The result gives ε_{th} of 15.55, which is much lower than the measured ε_r (18.01) by 15.8%. This may be related to the actual occupancy of ions, bond valence, and ion polarization. According to Brese's study [26], the bond valences of individual ions at the B-site are listed in Table 1. Clearly, the bond valence of Ti^{4+} with high ionic polarizability is only 3.49, significantly lower than its theoretical value of 4. Therefore, as the Ti-O bond length increases and Ti^{4+} has more vibrational space, it suggests that Ti^{4+} has a greater polarization. Thus, there is reason to believe that the ionic polarizability of Ti^{4+} ions may be significantly underestimated, resulting in the large gap between ε_r and ε_{th}. Based on the Clausius–Mosotti equation and the theory of ionic polarizability summation, the actual polarizability of Ti^{4+} ions in $Li_2Zn_6MgTi_6O_{20}$ ceramic is deduced to be 3.24, which exceeds Shannon's reported 2.93 $Å^3$ by 10.6%.

As shown in Fig. 5(b), the $Q\times f$ of $Li_2Zn_6MgTi_6O_{20}$ ceramic exhibits a rapid increase with temperature, reaching 98,450 GHz at 1240 °C, followed by a gradual decrease. This trend is consistent with the behavior of density and ε_r. In addition to external factors like relative density and second phase, intrinsic factors such as lattice vibration also significantly influence $Q\times f$. The packing fraction (P.F.) is commonly used to assess the intrinsic loss of ceramics, defined as the ratio of the total volume of packed ions inside the crystal to the unit cell volume [27]. Notably, P.F. and $Q\times f$ follow a similar pattern, where the highest P.F. values (63.67%) are linked to highest $Q\times f$ values at 1240 °C, indicating that a close atomic packing implies lower dielectric loss. This relationship holds true for $Zn_{2-2x}Li_xGa_{4+x}O_8$ [28] and $Ca_{1-x}Sr_xMgSi_2O_6$ [29] ceramics as well. The synergistic modulation of entropy plays a crucial role in enabling the ceramics to exhibit high $Q\times f$ values.

Raman spectra are commonly used for studying the local structure and lattice vibrational behavior of crystals. Fig. 6(a) illustrates the fitted Raman spectra of $Li_2Zn_6MgTi_6O_{20}$ ceramic at 1240 °C. According to the Raman polarization selection rule, a Zn_2TiO_4-type Raman spectrum with a typical disordered cubic inverse spinel structure is detected. The vibrational mode around 161 cm^{-1} may be due to the laser-induced plasma effect [30]. Previous literature [12] suggests that the observed mode at 387 cm^{-1} can be attributed to stretching vibrations in ZnO_4, which is also consistent with previous structural analyses. The additional broad peak at 588 cm^{-1} provides evidence for the disordered structure of the $Li_2Zn_6MgTi_6O_{20}$ ceramic [31]. The $A_{1\,g}$ vibrational mode at 775 cm^{-1} is associated with the stretching vibrations of the Ti-O bonds in the TiO_6 octahedra. The additional vibrational peak of 825 cm^{-1} arises from the random occupation of the octahedron by Li, Zn, Mg, Ti at B site. Additionally, the sharp shortening of certain bond lengths leads to the tilting of the TiO_6 octahedron to higher frequencies. The Raman spectra of other temperature ceramics are fitted with a Lorentzian function to determine the full width at half maximum (FWHM) of the $A_{1\,g}$ mode. The relationship between FWHM and the corresponding $Q\times f$ exhibits an opposite trend, as shown in Fig. 6(b). This is because a lower FWHM indicates smaller energy loss between

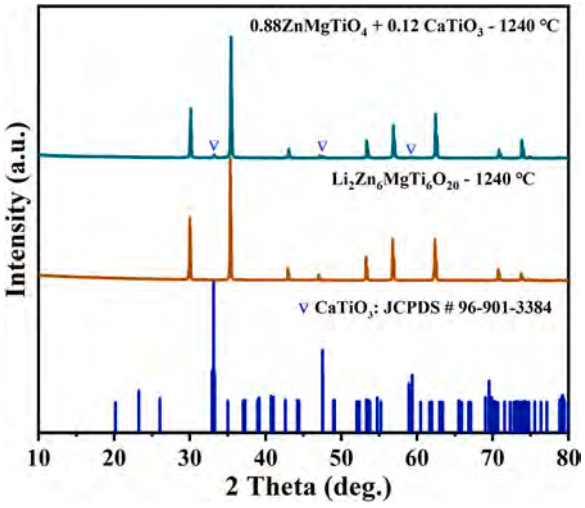

Fig. 8. XRD patternsof $0.88Li_2Zn_6MgTi_6O_{20} + 0.12CaTiO_3$ ceramic sintered at 1240 °C.

phonons, resulting in less dielectric loss. This phenomenon is also observed in materials such as $ZnMgTiO_4$ and $LiGa_5O_8$. This low dielectric loss is corroborated in the packing fraction and lattice energy.

The P–V–L chemical bond theory provides an effective framework for investigating chemical bond characteristics such as ionicity (f_i), lattice energy (U) and bond energy (E), and their interconnection with microwave dielectric properties [32]. Detailed calculation methods can be found in the Supplementary Information. Based on the obtained ionicity values of each bond (Table 1), the Ti-O bond features the highest f_i of 88.33%. This aligns with the fact that Ti^{4+} has a high ionic polarizability, which results in an increase in the ε_r. As shown in Fig. 7(a), the significant contribution of Ti^{4+} (73.32%) is responsible for the majority of U in $Li_2Zn_6MgTi_6O_{20}$ ceramic, which contributes to the dominant function of the ceramics in exhibiting low intrinsic dielectric losses. By analyzing the E of the ceramic, it is found that the contribution of the bond to the E at each position in the $Li_2Zn_6MgTi_6O_{20}$ is almost identical, which is most certainly due to the increased entropy value at the B site of the ceramic. This entropy effect also contributes to the fact that the $Li_2Zn_6MgTi_6O_{20}$ ceramics exhibit a superior comprehensive set of properties, including a lower sintering temperature, a higher $Q\times f$, and a nearer-zero τ_f (—38 ppm/°C), compared to ceramics such as Zn_2TiO_4, $ZnMgTiO_4$, and $Li_2ZnTi_3O_8$.

As shown in Fig. 6(d), the $Li_2Zn_6MgTi_6O_{20}$ ceramic exhibits a τ_f value of —38 ppm/°C at 1240 °C with minimal temperature dependence. To further enhance the utility of the ceramic, we investigated composite modulation by incorporating $CaTiO_3$ ceramics with a positive τ_f value. The XRD patterns, SEM image, and EDS result in Fig. 8 and Fig. S2 and clearly indicate the formation of two distinct phases in the

Table 2
Microwave dielectric properties of (1-x)$Li_2Zn_6MgTi_6O_{20}$-$x$$CaTiO_3$ composite ceramics (x represents bulk fraction).

x	S.T. (°C)	ε_r	$Q\times f$ (GHz)	τ_f (ppm/°C)
0	1240	18.01±0.2	98,450±3000	−38±3.6
0.08	1240	19.08±0.2	74,585±3000	−24.5±3.6
0.12	1240	19.54±0.2	53,674±2500	−4.5±3.6
0.16	1240	20.43±0.3	43,067±2500	+24.3±4.2

$0.88Li_2Zn_6MgTi_6O_{20}$ + $0.12CaTiO_3$ ceramic without any reactions, resulting in a stable composite ceramic. As summarized in Table 2, the $0.88Li_2Zn_6MgTi_6O_{20}$+$0.12CaTiO_3$ ceramic demonstrates excellent microwave dielectric properties at 1240 °C: ε_r = 19.54 ± 0.2, $Q\times f$ = 53,674 ± 2500 GHz, and τ_f = —4.5 ppm/°C + ± 3.6 ppm/°C.

4. Conclusion

In this study, the novel spinel $Li_2Zn_6MgTi_6O_{20}$ ceramic with high configuration entropy is synthesized with the solid-state method. The dense ceramic demonstrates a disordered state with space group *Fd*-3*m* and exhibits excellent microwave dielectric properties at 1240 °C: ε_r = 18.01 ± 0.2, $Q\times f$ = 98,450 ± 3000 GHz (at 9.17 GHz), and τ_f = −38 ± 3.6 ppm/°C. Further study shows that the ε_r of $Li_2Zn_6MgTi_6O_{20}$ is significantly higher than the ε_{th} due to the underestimation of 10.6% in the polarizability of the Ti^{4+} ion. Additionally, the P–V–L theory indicates that Ti^{4+} also contributes 73.32% to the U of the ceramic, which also plays an important role in the $Q\times f$ value. Remarkably, the introduction of the solid solution contributes to the disorder of the structure, which increases the conformational entropy and keeps the contribution of each bond to the bond energy in balance. This distinctive structural feature synergistically enhances the microwave dielectric properties and optimizes the sintering characteristics. Furthermore, the composite ceramic $0.88Li_2Zn_6MgTi_6O_{20}$+$0.12CaTiO_3$ is formed by compounding with $CaTiO_3$ to modulate the τ_f of the ceramic to near zero (—5.4 ± 3.6 ppm/°C) and obtain excellent overall performance (ε_r = 19.54 ± 0.2, $Q\times f$ = 53,674 ± 2500 GHz).

Author Statement

We wish to draw the attention of the Editor to the following facts which may be considered as potential conflicts of interest and to significant financial contributions to this work.

We confirm that the manuscript has been read and approved by all named authors and that there are no other persons who satisfied the criteria for authorship but are not listed. We further confirm that the order of authors listed in the manuscript has been approved by all of us.

We confirm that we have given due consideration to the protection of intellectual property associated with this work and that there are no impediments to publication, including the timing of publication, with respect to intellectual property. In so doing we confirm that we have followed the regulations of our institutions concerning intellectual property.

We understand that the Corresponding Author is the sole contact for the Editorial process (including Editorial Manager and direct communications with the office). He is responsible for communicating with the other authors about progress, submissions of revisions and final approval of proofs. We confirm that we have provided a current, correct email address which is accessible by the Corresponding Author and which has been configured to accept email from Hao Li, haouestc@gmail.com.

Declaration of Competing Interest

The authors declare that they have no known competing financial interests or personal relationships that could have appeared to influence the work reported in this paper.

Acknowledgments

This work was supported by the National Natural Science Foundation of China (No.52102129), the Hunan Provincial Natural Science Foundation of China (No.2023JJ30138) and the science and technology innovation Program of Hunan Province (2023RC3094).

Appendix A. Supporting information

Supplementary data associated with this article can be found in the online version at doi:10.1016/j.jeurceramsoc.2024.02.058.

References

[1] H.R. Tian, J.J. Zheng, L.T. Liu, H.T. Wu, H. Kimura, Y.Z. Lu, Z.X. Yue, Structure characteristics and microwave dielectric properties of $Pr_2(Zr_{1-x}Ti_x)_3(MoO_4)_9$ solid solution ceramic with a stable temperature coefficient, J. Mater. Sci. Technol. 116 (2022) 121–129.
[2] X. Zhou, L.T. Liu, J.J. Sun, N.K. Zhang, H.Z. Sun, H.T. Wu, W.H. Tao, Effects of $(Mg_{1/3}Sb_{2/3})^{4+}$ substitution on the structure and microwave dielectric properties of $Ce_2Zr_3(MoO_4)_9$ ceramics, J. Adv. Ceram. 10 (2021) 778–789.
[3] M.T. Sebastian, H. Jantunen, Low loss dielectric materials for LTCC applications: a review, Int. Mater. Rev. 53 (2008) 57–90.
[4] K. Du, X.Q. Song, J. Li, J.M. Wu, W.Z. Lu, X.C. Wang, W. Lei, Optimized phase compositions and improved microwave dielectric properties based on calcium tin silicates, J. Eur. Ceram. Soc. 39 (2019) 340–345.
[5] X. Zhang, B. Tang, Z. Fang, H. Yang, Z. Xiong, L. Xue, S. Zhang, Structural evolution and microwave dielectric properties of a novel $Li_3Mg_{2-x/3}Nb_{1-2x/3}Ti_xO_6$ system with a rock salt structure, Inorg. Chem. Front. 5 (2018) 3113–3125.
[6] Q.B. Du, Y. Tang, J. Li, W.S. Fang, A.H. Yang, J.Q. Chen, L. Fang, A low-εr and high-*Q* microwave dielectric ceramic Li_2SrSiO_4 with abnormally low sintering temperature, J. Eur. Ceram. Soc. 41 (2021) 7678–7682.
[7] L. Li, X.M. Chen, X.C. Fan, Microwave dielectric characteristics and finite element analysis of $MgTiO_3$–$CaTiO_3$ layered dielectric resonators, J. Eur. Ceram. Soc. 26 (2006) 3265–3271.
[8] H.H. Guo, M.S. Fu, D. Zhou, C. Du, P.J. Wang, L.X. Pang, W.F. Liu, A.S.B. Sombra, J.Z. Su, Design of a high-efficiency and-gain antenna using novel low-loss, temperature-stable $Li_2Ti_{1-x}(Cu_{1/3}Nb_{2/3})_xO_3$ microwave dielectric ceramics, ACS Appl. Mater. Interfaces 13 (2021) 912–913.
[9] Y.D. Zhang, D. Zhou, Pseudo phase diagram and microwave dielectric properties of Li_2O-MgO-TiO_2 ternary system, J. Am. Ceram. Soc. 99 (2016) 3645–3650.
[10] A. Belous, O. Ovchar, D. Durilin, M.M. Krzmanc, M. Valant, D. Suvorov, High-*Q* microwave dielectric materials based on the spinel Mg_2TiO_4,, J. Am. Ceram. Soc. 89 (2010) 3441–3445.
[11] W. Li, L. Fang, Y. Tang, Y.H. Sun, C.C. Li, Microwave dielectric properties in the $Li_{4+x}Ti_5O_{12}$ ($0 \le x \le 1.2$) ceramics, J. Alloy Compd. 701 (2017) 295–300.
[12] J. Zhang, R.Z. Zuo, Effect of ordering on the microwave dielectric properties of spinel-structured $(Zn_{1-x}(Li_{2/3}Ti_{1/3})_x)_2TiO_4$ ceramics, J. Am. Ceram. Soc. 99 (1) (2016) 7.
[13] Y.J. Wang, J. Li, W.S. Fang, Y. Tang, Z.Y. Zhang, L. Fang, A novel ultra-high Q microwave dielectric ceramic $ZnMgTiO_4$ with spinel structure, Ceram. Int. 49 (2023) 35420–35427.
[14] S. George, M.T. Sebastian, Synthesis and microwave dielectric properties of novel temperature stable high *Q*, $Li_2ATi_3O_8$ (A = Mg, Zn) ceramics, J. Am. Ceram. Soc. 93 (2010) 2164–2166.
[15] L. Fang, D.J. Chu, H.F. Zhou, X.L. Chen, Z. Yang, Microwave dielectric properties and low temperature sintering behavior of $Li_2CoTi_3O_8$ ceramic, J. Alloy. Compd. 509 (2011) 1880–1884.
[16] S.K. Singh, S.R. Kiran, V.R.K. Murthy, Raman spectroscopic and microwave dielectric studies on spinel $Li_2Zn_{(1-x)}Ni_xTi_3O_8$ compounds, Mater. Chem. Phys. 141 (2013) 822–827.
[17] B.B. Yang, Y. Zhang, H. Pan, W.L. Si, Q.H. Zhang, Z.H. Shen, Y. Yu, S. Lan, F. Q. Meng, Y.Q. Liu, H.B. Huang, J.Q. He, L. Gu, S.J. Zhang, L.Q. Chen, J. Zhu, C. W. Nan, Y.H. Lin, High-entropy enhanced capacitive energy storage, Nat. Mater. 21 (2022) 1074–1080.
[18] Q.S. Wang, A. Sarkar, D. Wang, L. Velasco, R. Azmi, S.S. Bhattacharya, T. Bergfeldt, A. Düvel, P. Heitjans, T. Brezesinski, H. Hahn, B. Breitung, Multi-anionic and -cationic compounds: new high entropy materials for advanced Li-ion batteries, Energy Environ. Sci. 12 (2019) 2433–2442.
[19] T. Löffler, H. Meyer, A. Savan, P. Wilde, A.G. Manjón, Y.T. Chen, E. Ventosa, C. Scheu, A. Ludwig, W. Schuhmann, Discovery of a multinary noble metal-free oxygen reduction catalyst, Adv. Energy Mater. 8 (2018) 1802269.
[20] Y.H. Ding, L. Liu, R.Z. Guo, L. Li, X.M. Chen, $(Hf_{0.25}Zr_{0.25}Sn_{0.25}Ti_{0.25})O_2$ high-entropy ceramics and their microwave dielectric characteristics, J. Am. Ceram. Soc. 105 (1) (2022) 8.
[21] D.Q. Chen, X.W. Zhu, S.Y. Xiong, G.B. Zhu, L.J. Liu, J. Khaliq, C.C. Li, Tunable microwave dielectric properties in rare-earth niobates via a high-entropy configuration strategy to induce ferroelastic phase transition, ACS Appl. Mater. Interfaces 15 (2023) 52776–52787.

[22] Q.B. Du, Y. Tang, J. Li, W.S. Fang, A.H. Yang, J.Q. Chen, L. Fang, A low-εr and high-Q microwave dielectric ceramic Li_2SrSiO_4 with abnormally low sintering temperature, J. Eur. Ceram. Soc. 41 (2021) 7678–7682.
[23] S. Buteea, A.R. Kulkarni, O. Prakasha, R.P.R.C. Aiyar, I. Wattamwar, D. Bais, K. Sudheendrand, K.C.James Raju, Significant enhancement in quality factor of Zn_2TiO_4 with Cu-substitution, Mater. Sci. Eng. B 176 (2011) 567–572.
[24] S.J. Penn, N.M. Alford, A. Templeton, X.R. Wang, M.S. Xu, M. Reece, K. Schrapel, Effect of porosity and grain size on the microwave dielectric properties of sintered alumina, J. Am. Ceram. Soc. 80 (1997) 1885–1888.
[25] R.D. Shannon, Dielectric polarizabilities of ions in oxides and fluorides, J. Appl. Phys. 73 (1993) 348–366.
[26] N.E. Brese, M. O'keeffe, Bond-valence parameters for solids, Acta Cryst. 47 (1991) 192–197.
[27] E.S. Kim, B.S. Chun, R. Freer, Effects of packing fraction and bond valence on microwave dielectric properties of $A^{2+}B^{6+}O_4$ (A^{2+}: Ca, Pb, Ba; B^{6+}: Mo, W) ceramics, J. Eur. Ceram. Soc. 30 (2010) 1731–1736.
[28] Y. Tang, Q.B. Du, H.C. Xiang, L. Fang, Tuning the order-disorder of $Zn_{2-2x}Li_xGa_{4+x}O_8$ spinel towards high-performance microwave dielectric ceramic, J. Alloy Compd. 927 (2022) 167026.
[29] C.Y. Cai, X.Q. Chen, H. Li, J. Xiao, C.W. Zhong, S.R. Zhang, Microwave dielectric properties of $Ca_{1-x}Sr_xMgSi_2O_6$ ceramics, Ceram. Int. 46 (2020), 27679–2768.
[30] K.R. Zhu, M.S. Zhang, Q. Chen, Z. Yin, Size and phonon confinement effects on low-frequency Raman mode of anatase TiO_2 nanocrystals, Phys. Lett. A 340 (2005) 220–270.
[31] Z. Wang, S.K. Saxena, C.S. Zha, In situ x-ray diffraction and Raman spectroscopy of pressure-induced phase transformation in spinel Zn_2TiO_4, Phys. Rev. B 66 (2002) 024103.
[32] H.Y. Yang, S.R. Zhang, H.C. Yang, E.Z. Li, Usage of P–V–L bond theory in studying the structural/property regulation of microwave dielectric ceramics: a review, Inorg. Chem. Front. 7 (2020) 4711–4753.